Research Square

Preprints are preliminary reports that have not undergone peer review.
They should not be considered conclusive, used to inform clinical practice,
or referenced by the media as validated information.

Study on fatigue life of orthotropic steel deck for urban rail transit based on fatigue model test and FEM modelling

Yong ZENG (yongzeng@cqjtu.edu.cn)
Chongqing Jiaotong University
Shenxu WANG
Chongqing Jiaotong University
Xiaofang XUE
Chongqing Jiaotong University
Hongmei TAN
Chongqing Jiaotong University
Jianting ZHOU
Chongqing Jiaotong University

Article

Keywords: Urban rail transit, orthotropic steel deck, fatigue testing, fatigue residual life, fatigue cracking, finite element method(FEM)

Posted Date: November 24th, 2022

DOI: https://doi.org/10.21203/rs.3.rs-2253956/v1

License: This work is licensed under a Creative Commons Attribution 4.0 International License.
Read Full License

Additional Declarations: No competing interests reported.

Study on fatigue life of orthotropic steel deck for urban rail transit based on fatigue model test and FEM modelling

Yong ZENG [1,2*], Shenxu WANG [1,2], Xiaofang XUE [1,2], Hongmei TAN [1,2]
Jianting ZHOU [1,2]

1 State Key Laboratory of Mountain Bridge and Tunnel Engineering, Chongqing Jiaotong University, Chongqing, 400074, China

2 Mountain Bridge and Materials Engineering Research Center of Ministry of Education, Chongqing Jiaotong University, Chongqing, 400074, China

Abstract: Orthotropic steel deck (OSD) structures are widely used in the bridge deck system of rail transit bridges. Reducing the amplitude of stress intensity factor is the most effective method to improve the fatigue life of OSD structures. In order to explore the fatigue crack propagation of OSD structure and the factors affecting the amplitude of structural stress intensity factor, linear elastic fracture mechanics and paris law is used for theoretical support in this paper. Firstly, a cable-stayed bridge of urban rail transit is taken as the research object, and a full-scale segment model of OSD structure is designed and static and fatigue tests are carried out. Based on the test data, the fatigue life of the structure is simulated and predicted. Finally, ABAQUS and Franc3D are used to analyze the influence of parameters, such as U-rib thickness, roof thickness and diaphragm thickness of OSD structure, on the amplitude of stress intensity factor. The test and FEM analysis results show that, the thickness of diaphragm and the height of U-rib have little effect on the fatigue life of OSD structure, appropriately increasing the thickness of top plate and U-rib has a positive significance for prolonging the fatigue life of the structure.

Key words: Urban rail transit; orthotropic steel deck; fatigue testing; fatigue residual life; fatigue cracking;finite element method(FEM)

1. Introduction

Nowadays, environmental protection and energy saving are more and more important, and urban rail transit has the advantages of being efficient, convenient, green and relieving congestion, etc. It has become one of the preferred modes of transport for most people. The deck plates of such structures are subjected to complex forces and are susceptible to fatigue cracking damage under high frequency fatigue cyclic loading.

Wu et al [1]used a Road rail dual-purpose arch bridge as a research object, determined the fatigue load spectrum parameters of the light rail support based on the actual light rail traffic, calculated the internal force history, and determined the constant fatigue load amplitude required for the fatigue test of three million cycles by using the linear cumulative damage criterion. Baietto et al [2]proposed a method to predict crack expansion by cross-validating the measured test values with the calculated values from finite element software analysis. Baietto et al [3]conducted fatigue tests on two sets of RD joint specimens with 15% and 75% weld penetration respectively in order to research the fatigue resistance around the rib plate (RD) weld in orthotropic steel bridge deck. Kainuma et al [4]monitored

the structural health of the Manhattan Bridge in real time based on FBG sensors, using deterministic and probabilistic methods to predict the remaining fatigue life of typical crack details, respectively. These studies are focused on the fatigue performance of orthotropic bridge deck of highway or railway steel bridges, while the research on orthotropic bridge deck of urban rail steel bridges is less. Especially the uniqueness of urban rail steel bridge structure and load.

In order to better understand the fatigue problems of orthotropic anisotropic plate structures for urban rail transit, a rail transit cable-stayed bridge is used as the background to study the fatigue design and cracking problems of this structure. Relying on the design model dimensions of an orthotropic anisotropic steel bridge deck structure for an urban rail transit cable-stayed bridge, and fatigue tests are carried out. Based on the fatigue cracking conditions of the tests, finite element expansion simulations of the cracks are carried out, and the remaining fatigue life of the structure is predicted based on the simulation results and compared with the results of the tests. The influence degree of the initial crack size, U-rib thickness, U-rib height, top plate thickness and cross partition thickness on the magnitude of the stress intensity factor at the leading edge of the cracks and the remaining fatigue life of the structure are investigated.

2. Fatigue crack expansion and analysis of calculation results

2.1 Calculation of the stress intensity factor

The cross-integration method (M-integration) is used to calculate the stress intensity factors. The cross-integration method enables the calculation of stress intensity factors for isotropic materials and generally anisotropic materials with type I, II and III cracks (K_{I}, K_{II} and K_{III}). The calculation principle of interactive integration is as follows :

Based on the fracture mechanics, it can be integrated as:

$$J=\lim_{\Gamma_s\to 0}\int_{\Gamma_s}(w\delta_{ij}-\sigma_{ij}u_{ij})n_j\mathrm{d}\Gamma \tag{1}$$

Where n_j is the vector of the outer normal, Γ_{S} to the crack tip perimeter, and Γ_{S} is shown in Fig.1.

w is expressed as the strain energy density with the following expression:

$$w=\frac{1}{2}\sigma_{ij}\varepsilon_{ij}^{m} \tag{2}$$

Where ε_{ij}^{m} indicates partial strain.

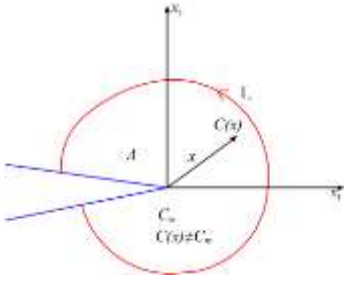

Fig.1 Integral contour

Rewriting the above J integral into a domain integral, then:

$$J = \int_A (\sigma_{ij} \frac{\partial u_i}{\partial x_1} - w\delta_{1j}) \frac{\partial q}{\partial x_j} \mathrm{d}A + \int_A (\sigma_{ij} \frac{\partial u_i}{\partial x_1} - w\delta_{1j}) q \mathrm{d}A \tag{3}$$

Where q indicates the crack expansion vector.

Superimposing the real stress field around the crack with the auxiliary fields ($u^{aux}, \sigma^{aux}, \varepsilon^{aux}$)on each other to obtain:

$$\begin{aligned} J^S = &\int_A \left\{ (\sigma_{ij} + \sigma_{ij}^{aux})(\frac{\partial u_i}{x_1} + \frac{\partial u_i^{aux}}{x_1}) - \frac{1}{2}(\sigma_{ik} + \sigma_{ik}^{aux})(\varepsilon_{ik} + \varepsilon_{ik}^{aux})\delta_{1j} \right\} \frac{\partial q}{\partial x_1} \mathrm{d}A \\ &+ \int_A \left\{ (\sigma_{ij} + \sigma_{ij}^{aux})(\frac{\partial u_i}{x_1} + \frac{\partial u_i^{aux}}{x_1}) - \frac{1}{2}(\sigma_{ik} + \sigma_{ik}^{aux})(\varepsilon_{ik} + \varepsilon_{ik}^{aux})\delta_{1j} \right\} q \mathrm{d}A \end{aligned} \tag{4}$$

M can be rewrited as the interaction credit:

$$\begin{aligned} M = &\int_A \left\{ \sigma_{ij} u_{i,1}^{aux} + u_{i,1} \sigma_{ij}^{aux} - \frac{1}{2}(\sigma_{ik}\varepsilon_{ik}^{aux} + \sigma_{ik}^{aux}\varepsilon_{ik}^{m})\delta_{1j} \right\} q_{,j} \mathrm{d}A \\ &+ \int_A \left\{ \sigma_{ij} u_{i,1}^{aux} + u_{i,1} \sigma_{ij}^{aux} - \frac{1}{2}(\sigma_{ik}\varepsilon_{ik}^{aux} + \sigma_{ik}^{aux}\varepsilon_{ik}^{m})\delta_{1j} \right\} q \mathrm{d}A \end{aligned} \tag{5}$$

Substituting the split-tip auxiliary field A into the above equation, then:

$$\begin{aligned} M = &\int_A \left\{ \sigma_{ij} u_{i,1}^{aux} + u_{i,1} \sigma_{ij}^{aux} - \sigma_{ik}\varepsilon_{ik}^{aux} \right\} q_{,j} \mathrm{d}A \\ &+ \int_A \left\{ \sigma_{ij} u_{i,1}^{aux} + u_{i,1} \sigma_{ij}^{aux} - \sigma_{ik}\varepsilon_{ik}^{aux} \right\} q \mathrm{d}A \end{aligned} \tag{6}$$

According to equations (1) and (3), equation (6) can be expressed as

$$J^S = J + J^{aux} + M \tag{7}$$

For open cracks, the relationship between the M integral and the Type I stress intensity factor is

$$\begin{aligned} M &= \frac{2}{E^*} K_{\mathrm{I}} K_{\mathrm{I}}^{aux} \\ K_{\mathrm{I}} &= \frac{E^*}{2} M \end{aligned} \tag{8}$$

Where $K_{\mathrm{I}}^{aux} = 1$.

For plane strain state, $E^* = E/(1-v^2)$, where v indicates the possion ration.

The normalized stress intensity factor($K_{\mathrm{I}}, K_{\mathrm{II}}$ and K_{III})calculation results of the initial crack front are shown in Fig.2. The calculation at the position 0.5 corresponds to the calculated value of

the stress intensity factor at the deepest point in the short semi-axis of the semi-elliptical crack and SIF represents the stress intensity factor value.

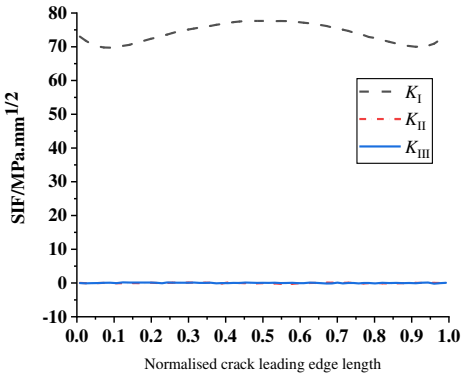

Fig.2 Normalized stress intensity factor at initial crack front

As can be seen from Fig.2, the initial crack type I stress intensity factor is symmetrically distributed, with larger values at the middle of the crack leading edge (short semi-axial crack tip) and at the ends of the long semi-axis, with a maximum value of up to 77.67 MPa.mm1/2, which shows that the initial crack expands relatively quickly at the ends of the long and short semi-axes; and the stress intensity factors of type II and type III fluctuate around 0 MPa.mm1/2, which is much smaller than the stress intensity factors for Type II and Type III fluctuate around 0 MPa.mm and are much smaller than those for Type I. It shows that the crack is a composite crack dominated by Type I cracks.

2.2 Fatigue life assessment method based on fracture mechanics

In the assessment of the fatigue life of metallic structures, many researches have been done and a lot of achievements have been made. Based on the fatigue crack expansion of metallic materials, the mathematical model of fatigue crack expansion as shown in Fig.3 was obtained[5].

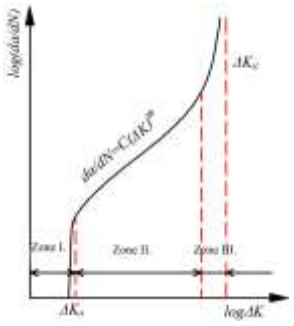

Fig.3. Fatigue crack expansion curves

As can be seen from Fig.3, crack expansion can be divided into three stages. When the crack tip's stress intensity factor amplitude value, ΔK, is less than the threshold value, ΔK_{th}, the crack is in the first stage, and the crack does not expand. When the crack tip's ΔK is higher than ΔK_{th}, the crack is in the second stage, and the crack will gradually and smoothly expand, which is currently described by the Paris law for this stage of crack expansion. When the crack tip's ΔK is

close to ΔK_{IC}, the crack is in the third stage , and it expands rapidly and fractures unsteadily.

In this paper, Paris law will be used to estimate the fatigue life of components, Paris law is as follows[6]:

$$da / dN = C(\Delta K)^m \tag{9}$$

Where N is the number of stress cycles; $\Delta K = K_{\max} - K_{\min}$ is the amplitude value of the stress intensity factor; $K_{\max}$、$K_{\min}$ are the maximum and minimum values of K under cyclic loading, respectively; and C and m represent the material parameters associated with the test conditions.

Integrating equation (9) over the crack length a, an expression for the remaining fatigue life of the member can be got.

$$N = \int_{a_0}^{a_{cr}} \frac{1}{C(\Delta K)^m} da \tag{10}$$

Where a_0 is the initial crack length, and a_{cr} is the critical crack length.

When m = 2, the expression for calculating the remaining life of a fatigue crack is

$$N = \frac{1}{C(\Delta K)^m} \ln(\frac{a_{cr}}{a_0}) \tag{11}$$

When m $\neq$ 2, the expression for calculating the remaining life of a fatigue crack is

$$N = \frac{1}{C(\Delta K)^m (0.5m-1)} (a_0^{1-0.5m} - a_{cr}^{1-0.5m}) \tag{12}$$

The Paris law is simple and has a small margin of error, and is one of the most commonly used formulas for predicting the remaining fatigue life of a steel component.

2.3 Simulation of crack extension

Three-dimensional crack growth is predicted in the following steps:

1) The local torsion angle can be calculated based on the stress at the leading edge of the local crack in the local co-ordinate system shown in Fig.4, where the stress is determined by the local stress intensity factor.

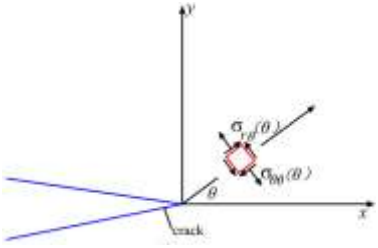

Fig.4 Local crack leading edge stress

2) Solve for the length of the local extension at each point.

The leading edge of the new crack after extension is smoothly smoothed and the leading edge of the crack is externally inserted outside the free surface of the structure.

A schematic diagram of the predicted crack front in Franc3D is shown in Fig.5.

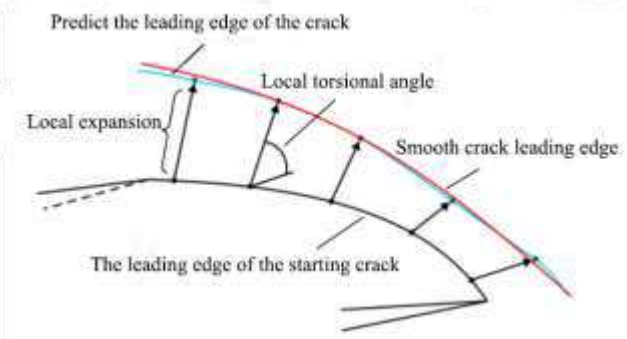

Fig.5 Schematic diagram of crack front prediction

2.4 The steps of calculating fracture parameters by finite element method

Fatigue crack growth and fracture parameters are conducted by finite element method as follows:

(1) Building the finite element model

In finite element software (e.g. ABAQUS), the whole model without cracks is created. To increase the speed of calculation, the elements in the crack extension area are usually set into a group defined as a sub-model, and the non-crack extension area is defined as the key pattern.

(2) Introduction of initial cracking

The shape and size of the initial crack are inserted into the sub-model according to the operation flow of the new defect wizard, and the mesh are regenerated.

(3) Finite element calculation

The cracked sub-model is reassembled with the master pattern as a whole model containing the cracks, and is automatically submitted to the finite element software for calculation.

(4) Prediction of crack growth

The stress results and the stress intensity factors of each node at the crack front are read, the expansion step or the number of cyclic load actions are set, the position of the crack front are updated, and the mesh of the sub-model is .remeshed.

(5) Performing new finite element calculations

When the obtained results do not meet the user-defined stop conditions, the crack front position will continue to be updated and calculated. If the obtained results meet the user-defined stop conditions, the propagation analysis will be completed.

3. Model design of fatigue test

3.1 Model design

The test is based on an urban rail transit cable-stayed bridge with a main span of 340m. The size of the model is designed according to the structural size of the steel deck of the bridge, and the model is simplified according to the actual situation. Q345qD steel material is used as the model material. Three U-ribs with a spacing of 600mm are set in the transverse bridge direction, and three

diaphragm plates with a spacing of 827mm are set in the longitudinal bridge direction. The 12mm-thick steel plates are used at both ends for heads, and the size is 1800mm×121mm×281mm.The steel box is placed at the lower part of both ends of the bridge deck and used as a support to keep the deck horizontal. The overall dimension of the model is 3000mm×1800mm, and the thickness of the deck, diaphragm and U-shaped longitudinal rib is 16mm, 12mm and 8mm, respectively. Since the restraints between the diaphragm and the U-rib will produce secondary bending stress, in order to reduce this stress, appropriate notches are usually made at the intersection between the lower part of the U-rib and the diaphragm, and the notch radius of the model designed for this fatigue test is 25mm. The front view and three-dimensional view of the model are shown in Fig.6 and Fig.7, respectively.

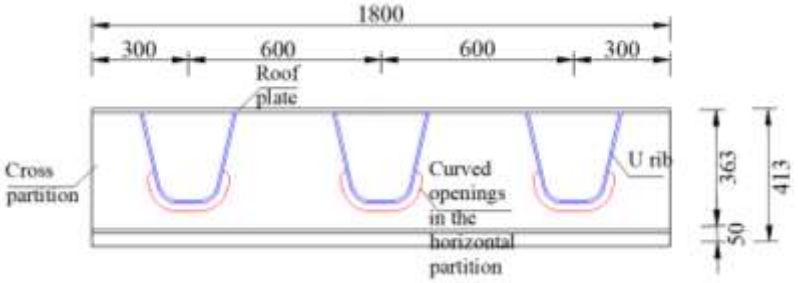

Fig.6 Front view of the full-Scale Model/mm

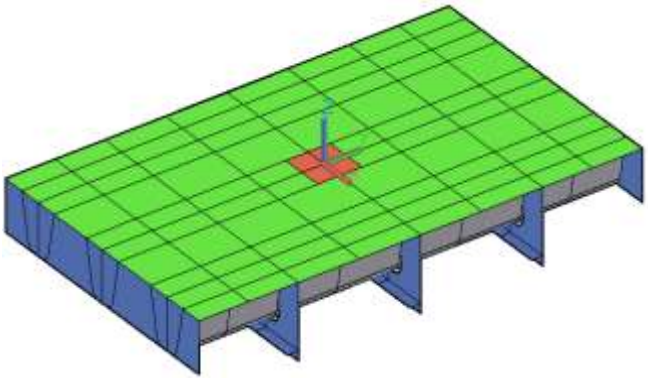

Fig.7 Three-dimensional view of the full-Scale sectional test Model

3.2 Layout of measuring points

In order to investigate the stress and fatigue performance of OSD of test model, strain measuring points are arranged at the joint of longitudinal ribs and diaphragms, the joint of longitudinal ribs and top plates and the edges of diaphragm openings. The measuring point numbers of the middle diaphragm, side diaphragms, longitudinal ribs and top plates are ZHGB1-1 to ZHGB1-35, BHGB1-1 to BHGB1-19, BHGB2-1 to BHGB2-5, U1 to U6 and P1 to P6,respectively. The strain gauges used in this test were BX120-3CA, with a sensitive grid size of 3mm×2mm and a resistance of 120 Ω±0.1%. A total of 71 strain gauges were laid out for the test, of which 35 were laid out in the middle cross partition, 19 in the side cross partition 1 (BHGB1), 5 in the side cross partition 2 (BHGB2) which was symmetrical to BHGB1, and 6 in the U-rib and 6 in the top plate. The specific location of the measurement points is shown in Fig.8, where the black numbers in Fig.8(a) indicate the location of the intermediate measurement points, the red numbers in brackets indicate the location of the side bulkhead 1 (BHGB1) measurement points and the blue numbers

indicate the location of the side bulkhead 2 (BHGB2) measurement points.

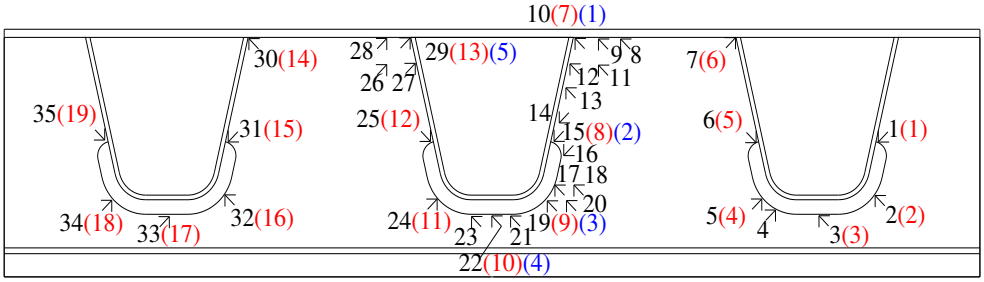

(a) Layout of measuring points of the middle diaphragm

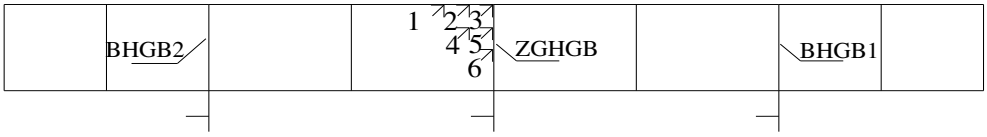

(b) Layout of U-rib measuring points

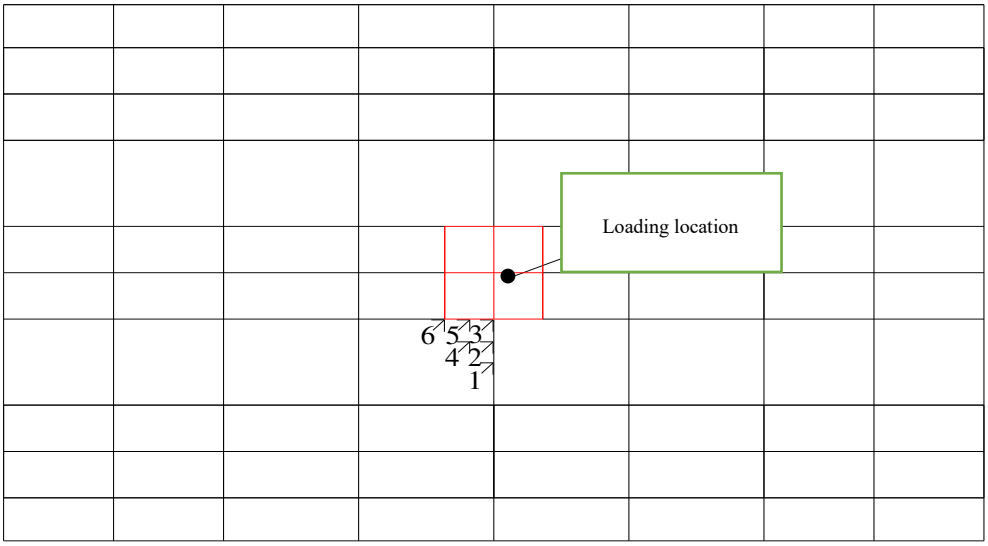

(c) Layout of roof measuring points

Fig.8 Layout of measuring points

4. Fatigue test results

4.1 Static load test results

Before the static load test, the strain gauges are checked for adhesion and the strain gauges are in good condition, after which at least 3 preloads are carried out and data collected. The loading principle of static load test is to load step by step from zero to the maximum static load value, and then all loads are removed symmetrically. After each load, a three-minute pause was taken to collect strain and displacement data. The maximum value of the static load for this test is 131.6kN and the whole loading process is 0kN, 10kN, 30kN, 70kN, 110kN, 131.6kN, 110kN, 70kN, 30kN, 10kN, 0kN, respectively. The above steps are operated at least twice, and the average values are calculated

in order to reduce the dispersion of the test data.

The comparison results between measured values and calculated values of some key test points are listed in Tab.1.

Tab.1 Comparison of measured and calculated values at selected measurement points under static load

Location	Measurement points	Measured values/MPa	Calculated values/MPa
Roof plates	P2	56.6	55.5
	P3	156.6	160.1
	P4	112.7	113.3
U ribs	U2	53.4	55.0
	U3	64.7	63.9
	U4	36.6	35.2
Side dividers 1	BHGB1-6	9.3	9.6
	BHGB1-8	12.4	11.9
	BHGB1-10	14.2	14.5
	BHGB1-12	11.5	12.6
	BHGB1-14	6.3	6.8
Mid-transom bulkhead	ZHGB1-7	29.0	29.3
	ZHGB1-9	39.8	40.2
	ZHGB 1-15	52.9	53.5
	ZHGB 1-25	54.0	54.2
	ZHGB 1-31	19.3	20.6
	ZHGB1-35	11.1	12.8

4.2 Fatigue test process

The fatigue load range for this test is from 10 kN to 131.6 kN. When the cyclic loading times reach 50000 times, 250000 times, 500000 times, 750000 times, 1000000 times, 1250000 times, 150000 times, 750000 times and 2000000 times, respectively, the machine is stopped for static load test, the strain values and displacement values are measured, and the model is checked.

If the test specimen is still in good condition when the number of loadings reach two million, the load amplitude is increased and the fatigue test is continued. When the loading times reach 2.25 million times, 2.5 million times, 2.75 million times, 3.0 million times, 3.25 million times, 3.5 million times, respectively. The test is stopped and the strain and displacement values are measured and the condition of the model is checked. If the specimen has not been damaged after 3.5 million cycles of loading, the test is stopped. The fatigue load test process is shown in Fig.9.

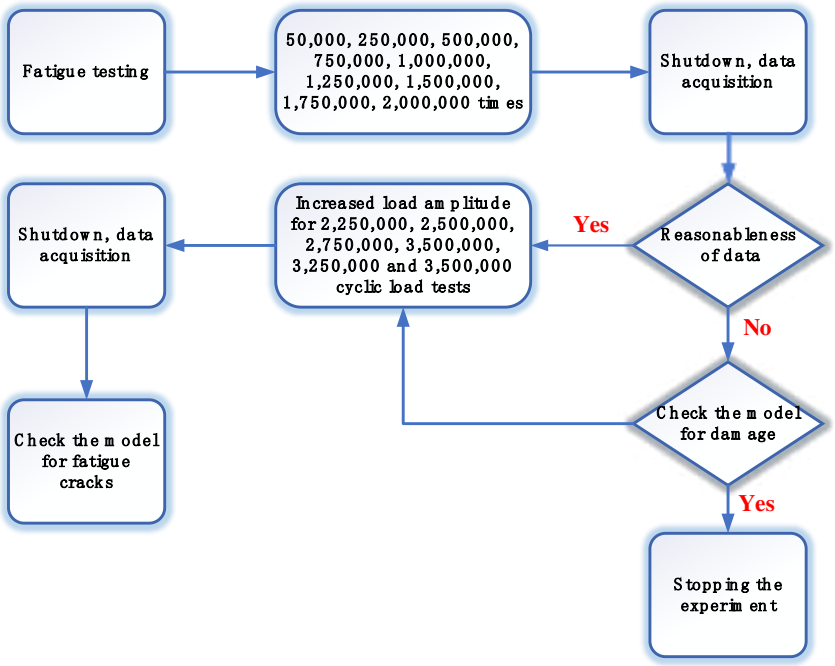

Fig.9 Flow chart of fatigue load test

4.3 Fatigue cracking's location

At the completion of 2 million cycles of loading, the fatigue load amplitude was 121.6kN, and no fatigue crack was found after careful observation. At 2 million to 2.5 million and 2.5 million to 3 million cycles, the fatigue load amplitude was increased to 1.25 and 1.5 times the original one, respectively, and no crack visible to the naked eye appeared on the test model. At 3 million to 3.25 million cycles, the fatigue load amplitude went to 1.75 times the original one, and a crack of 15.1cm in length appeared near the boundary of the loading location. At 3.25 million to 3.5 million cycles, a crack of 18.6cm appeared. The fatigue cracks in the test model are shown in Fig.10.

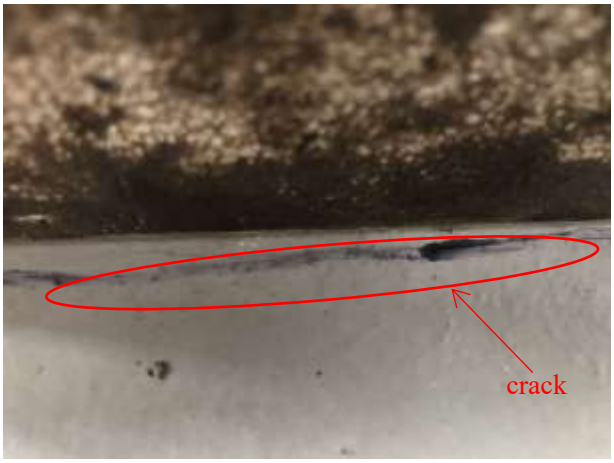

Fig.10 Schematic diagram of fatigue crack location

5. Fatigue crack life prediction

5.1 Fatigue cracking modelling

From the test results, it can be seen that the cracks appear at the junction of the top plate - U-rib

- middle diaphragm and crack downwards from the top surface of the top plate, so this section is devoted to an extended analysis of the cracks at this point. According to the study of fatigue cracking by Ya et al [7], Chen Chuanyao, Liu Yanping et al [8], the shape of the fatigue crack can usually be approximated as a semi-ellipse, and it is assumed in this section that the initial half short axis of the crack is 0.1mm and the half long axis is 0.15mm; the structure is considered to be damaged when the depth of the crack penetrates the top plate, and the corresponding number of cyclic loads is the fatigue residual life of the OSD model structure.

ABAQUS modelling software is used to build a whole model without initial crack, and the load and boundary conditions of the whole model are the same as the test model. The model and calculation results are shown in Fig.11~14. The elements in the crack extension area are set into a group and defined into a sub-model, then the model is imported into Franc3D, so an initial crack is inserted into the sub-model and the mesh is regenerated. At this time, the leading edge of the crack is divided into three rings of elements with a radius of one tenth of the short semi-axis of the crack. The initial crack front mesh division is shown in Fig.15. Finally, the sub-model and the key pattern are reassembled into a model with the crack, and are submitted together to ABAQUS for finite element calculations.

Fig.11 Geometric model

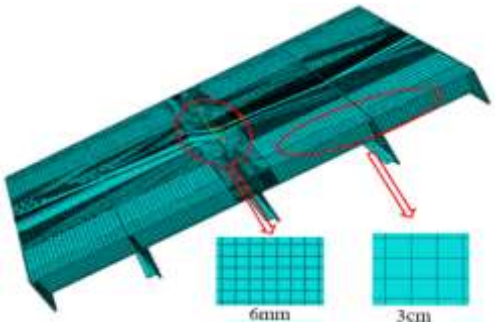

Fig.12 Finite element model

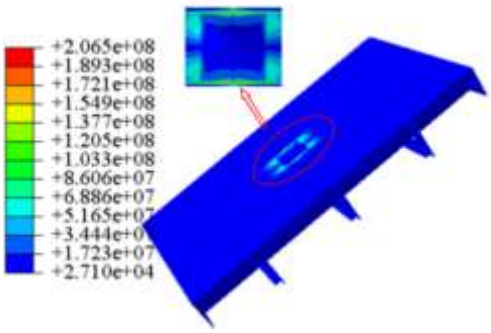

Fig.13 Finite element Von-Mises stress nephogram/Pa

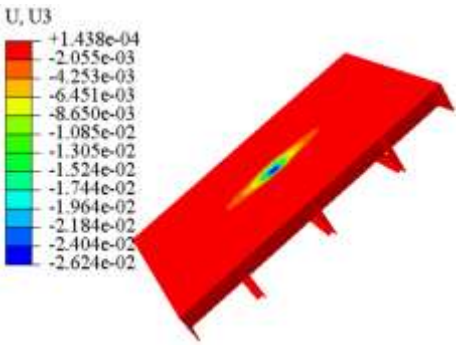

Fig.14 Finite element vertical displacement nephogram/m

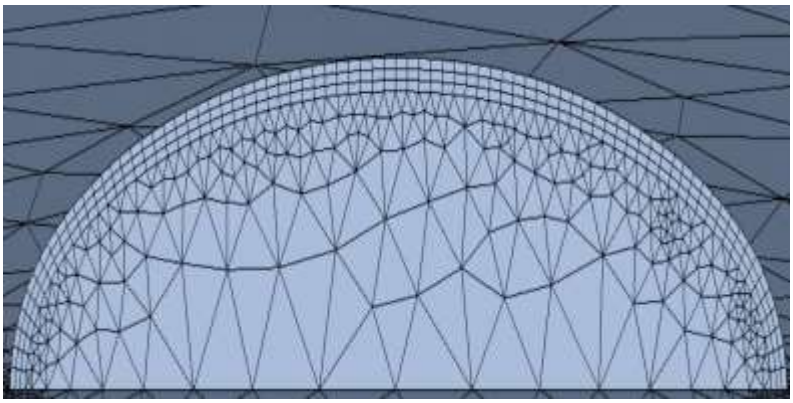

Fig.15 Meshing of crack front of the model

The normalized stress intensity factor(K_{I} , K_{II} and K_{III})calculation results of the initial crack front are shown in Fig.16, The calculation at the position 0.5 corresponds to the calculated value of the stress intensity factor at the deepest point in the direction of the short semi-axis of the semi-elliptical crack, and SIF represents the stress intensity factor value.

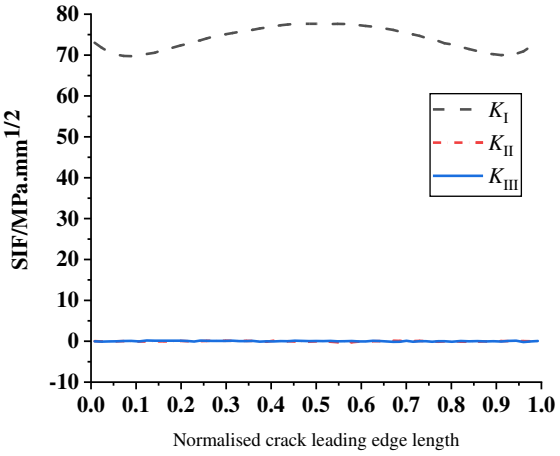

Fig.16 Normalized stress intensity factor at initial crack front

As can be seen from Fig.16, the initial crack type I's stress intensity factor is symmetrically distributed, with larger values at the middle of the crack leading edge (short semi-axial crack tip), and at the ends of the long semi-axis, with a maximum value of up to 77.67 MPa.mm$^{1/2}$, which shows that the initial crack expands relatively quickly at the ends of the long and short semi-axes. The stress intensity factors of type II and type III fluctuate around 0 MPa.mm$^{1/2}$, which is much smaller than the stress intensity factors for Type II and Type III fluctuate around 0 MPa.mm, and both are much smaller than those for Type I. This shows that the crack is a crack dominated by Type I cracks.

Typically, the extension step for each node on the leading edge of the crack is different. Two methods of calculating the extension step are provided in Franc3D software. One is to specify the extension step for the node located at the median value of the stress intensity factor, and the extension step for all other nodes is obtained by appropriate scaling, and the other is to specify the number of cycles of the load and solve directly for the extension step for each node according to the

Paris law. In this section, the former method was used to calculate the expansion step for the nodes on the leading edge of the crack, specifying the expansion step at the median stress intensity factor to be less than or equal to fifteen percent of the characteristic size of the crack, for a total of 37 expansion steps.

The specific extension step lengths for each step are shown in Tab.2, and the crack changes throughout the extension process are shown in Fig.17 to 23. Due to the relatively large number of extension steps, only the crack changes for some key extension steps are shown.

Tab.2 Crack extension sizes per step

Extension steps	Current size/mm	Extended step size/mm	Extension steps	Current size/mm	Extended step size/mm
0	0.100	0.015	19	1.424	0.213
1	0.115	0.017	20	1.637	0.245
2	0.132	0.020	21	1.882	0.282
3	0.152	0.023	22	2.164	0.325
4	0.175	0.026	23	2.489	0.373
5	0.201	0.030	24	2.863	0.429
6	0.231	0.035	25	3.292	0.494
7	0.266	0.040	26	3.786	0.568
8	0.306	0.046	27	4.354	0.653
9	0.352	0.053	28	5.007	0.751
10	0.405	0.061	29	5.758	0.864
11	0.465	0.070	30	6.621	0.993
12	0.535	0.080	31	7.614	1.142
13	0.615	0.092	32	8.757	1.313
14	0.708	0.106	33	10.070	1.510
15	0.814	0.122	34	11.580	1.737
16	0.936	0.140	35	13.318	1.341
17	1.076	0.161	36	14.659	1.341
18	1.238	0.186	37	16.000	/

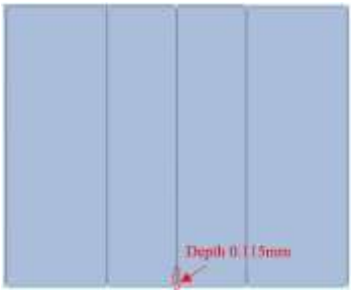

(a) Side view of the crack

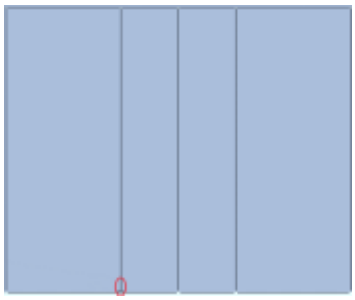

(b) Front view of the crack

Fig.17 Crack shape simulation in Step 1

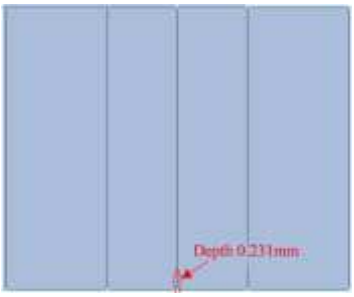

(a) Side view of the crack

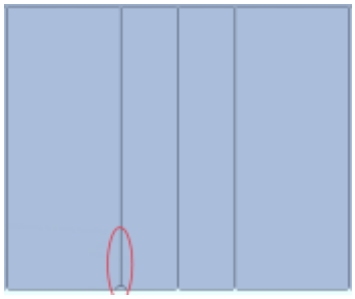

(b) Front view of the crack

Fig.18 Crack shape simulation in Step 6

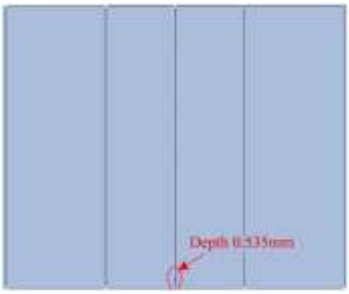

(a) Side view of the crack

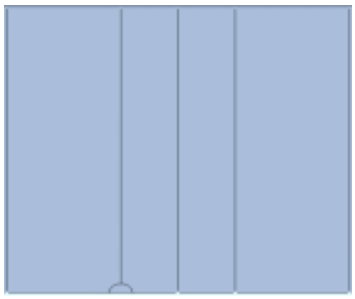

(b) Front view of the crack

Fig.19 Crack shape simulation in Step 12

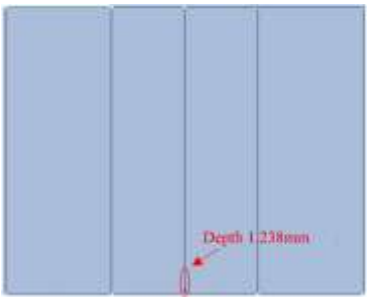

(a) Side view of the crack

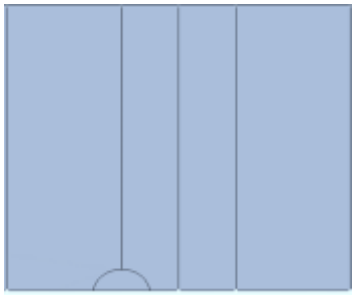

(b) Front view of the crack

Fig.20 Crack shape simulation in Step 18

(a) Side view of the crack

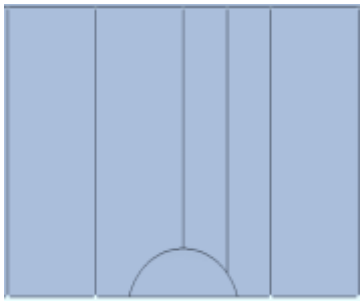

(b) Front view of the crack

Fig.21 Crack shape simulation in Step 24

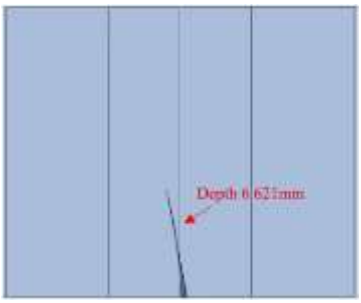

(a) Side view of the crack

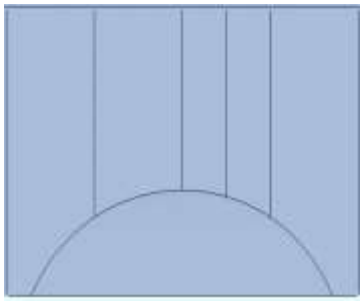

(b) Front view of the crack

Fig.22 Crack shape simulation in Step 30

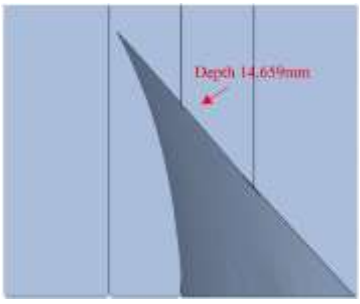

(a) Side view of the crack

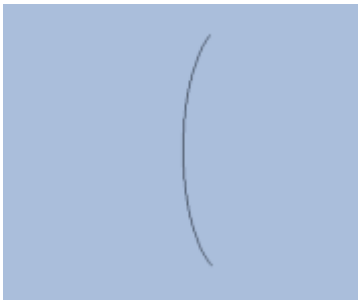

(b) Top view of the crack

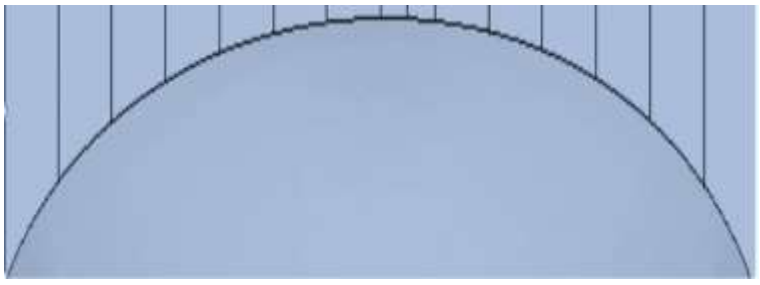

(c) Front view of the crack

Fig.23 Crack shape simulation in Step 36

The stress intensity factor for each key extension step was calculated using the method of

calculating the stress intensity factors for the initial crack, and the results are shown in Fig.24. Due to the large number of extension steps, only some of the extension steps are listed in Fig.24.

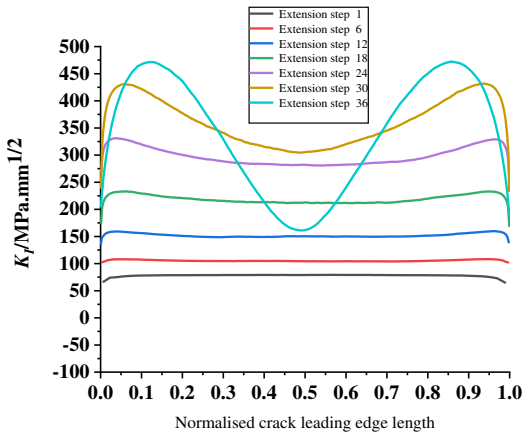

Fig.24 Calculation of stress intensity factors for the leading edge of some extended-step cracks

According to Fig.24, the stress intensity factor at the middle point of the leading edge of the crack is larger than the other points when the crack is first expanded, so the expansion rate at this point is relatively large. With the increases of the expansion steps, the stress intensity factors at about 5%-10% from the two end points of the long half-axis are obviously larger than the stress intensity factors at other points, so the expansion rate of the crack along the long half-axis is larger than the expansion rate along the short half-axis. At the same time, as the crack expands, the stress intensity factor at the middle point of the leading edge of the crack shows a trend of firstly increasing and then decreasing. The reason for this phenomenon may be the fact that the crack expansion in the length direction is based on the expansion fitting in the depth direction, which makes the expansion rate in both directions slightly different, which in turn may lead to an increase in the ratio of the long semi axis to the short semi axis in the expansion process, and the gradual flattening of the crack shape,which is no longer stable,also causes a change in the stress intensity factor at the mid-point of the leading edge of the crack. The observation of the model test shows that the cracks are indeed very flat and long semi-elliptical in shape,which shows that the expansion of the fatigue cracks is objective and inevitablely related to the special stress pattern of the OSD structure. The variation in length and direction of crack long and short semi-axes during the whole expansion process is shown in Fig.25.

(a) Crack growth variation of long half axis (b) Crack growth change of short half axle

Fig.25 Crack growth changes of long and short half axes

5.2 Life expectancy

The relationship between the number of cyclic loads and the size of the crack in the short half-axis is calculated and shown in Fig.26.

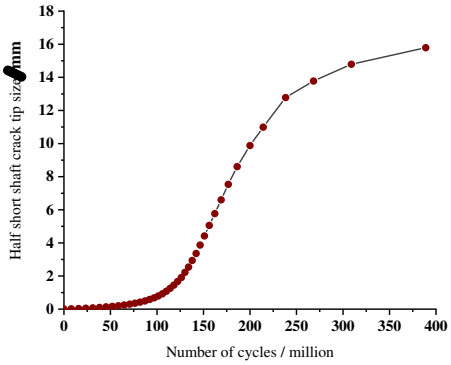

Fig.26 Relationship between cyclic load times and crack size of short half axis

As can be seen from Fig.26, when the crack short half axis size reaches 16mm, the number of load cycles is nearly 3.9 million. That is, the fatigue life of the OSD model structure is about 3.9 million, while the number of fatigue cycle loads obtained from the test is nearly 3.5 million, with a relative error of 11.4%, which is within an acceptable range. The relative error between the model test and the FEM simulation results is inevitable as the effects of objective factors, because crack closure effects are not taken into account in the simulation of crack expansion, and the expansion parameters C and m are estimated, whereas in practice the values of C and m are different for different materials, different crack shapes and different stress ratios.

6. Influences of different parameters on residual life of structure

The crack fatigue life of OSD [7]may be affected by the initial defect size, the thickness and height of U-rib, the thickness of top plate and the thickness of diaphragm. Therefore, the method combining ABAQUS and Franc3D is used to analyze the influence of various parameters on the crack life, providing a reference for the future design of this kind of OSD structure.

6.1 Initial crack size

Because the OSD structure is very complex, coupled with environmental and manufacturing factors, it is inevitable to produce initial defects. Generally, the initial crack size can be obtained by nondestructive evaluation method or equivalent initial defect size method. In order to investigate the effect of the initial crack size on the remaining fatigue life of the OSD structure, the stress intensity factor amplitude ΔK_{I} at the midpoint of the leading edge of the initial crack (tip of the short semi-axis) and the number of cyclic loads required to damage the structure (remaining fatigue life of the structure) are calculated for different sizes at a ratio of 3/2 between the long and short semi-axes. The relationship between the propagation depth of the middle point of the crack front and the amplitude of the stress intensity factor(ΔK_{I}) is shown in Fig.27, and the relationship between the propagation depth of the middle point of the crack front and the number of cyclic loads is shown in Fig.28.

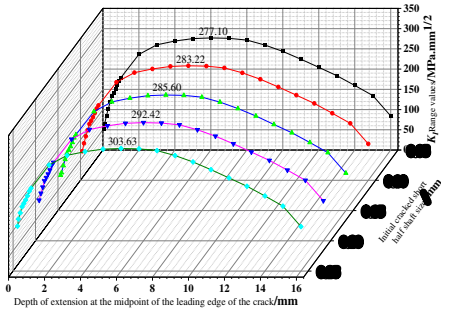

Fig.27 The relationship between the propagation depth at the middle point of crack front and the amplitude of stress intensity factor

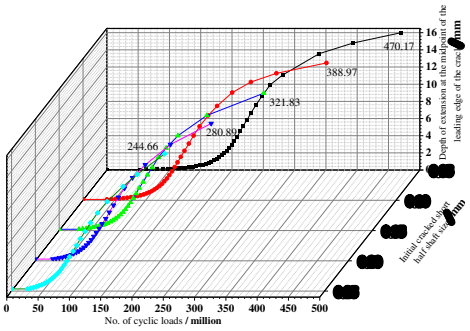

Fig.28 The relationship between the propagation depth at the middle point of crack front and the number of cyclic loading

From the above two figures, it can be seen that the amplitudes of the stress intensity factor at the middle point of the crack front during the propagation of the initial cracks have the same shape, showing a trend of first increasing and then decreasing. The smaller the initial crack size is, the smaller the stress intensity factor amplitude at the crack front is, and the larger the residual fatigue life is.

6.2 Thickness of U-rib

The different thickness of the U-rib and all other constant parameters are studied. The relationship between the propagation depth of the middle point of the crack front and the amplitude of the stress intensity factor(ΔK_1) is shown in Fig.29, and the relationship between the propagation depth of the middle point of the crack front and the number of cyclic loads is shown in Fig.30.

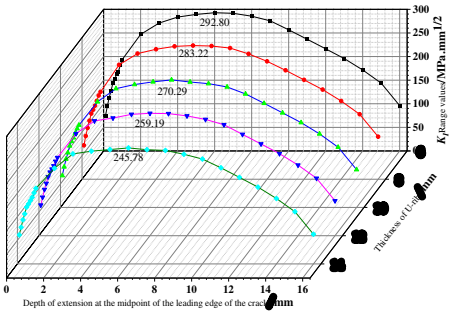

Fig.29 The relationship between the propagation depth at the middle point of crack front and the amplitude of stress intensity factor

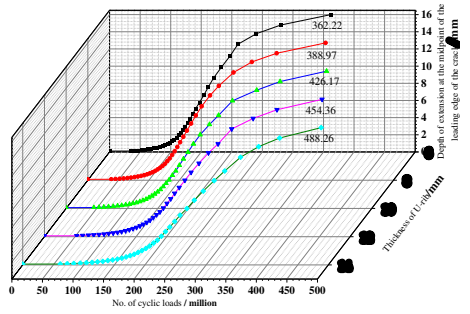

Fig.30 The relationship between the propagation depth at the middle point of crack front and the number of cyclic loading

It can be seen from the above two figures that the thickness of U-rib has a certain impact on the service life of the OSD structure. That is, with the increase of the thickness of U-rib, the amplitude of stress intensity factor at the middle point of crack front decreases, and the fatigue life of the structure increases. This is probably due to the fact that the increase in U-rib thickness increases the stiffness of the structure as well as the load carrying capacity, therefore, an appropriate increase in U-rib thickness can improve the service life of the structure while taking into account economic factors.

6.3 U-rib height

Simulation of the test model by the different height of the U-rib and other constant parameters are performed. The relationship between the propagation depth of the middle point of the crack front and the amplitude of the stress intensity factor(ΔK_{I}) is shown in Fig.31, and the relationship between the propagation depth of the middle point of the crack front and the number of cyclic loads is shown in Fig.32.

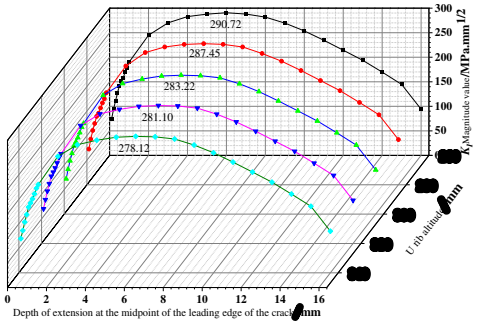

Fig.31 The relationship between the propagation depth at the middle point of crack front and the amplitude of stress intensity factor

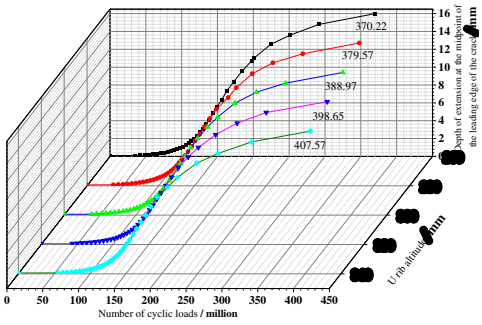

Fig.32 The relationship between the propagation depth at the middle point of crack front and the number of cyclic loading

6.4 Thickness of top plate

Simulation of the test model by the different thickness of the top plate and all other constant parameters are conducted. The relationship between the propagation depth of the middle point of the crack front and the amplitude of the stress intensity factor(ΔK_{I}) is shown in Fig.33, and the relationship between the propagation depth of the middle point of the crack front and the number of cyclic loads is shown in Fig.34.

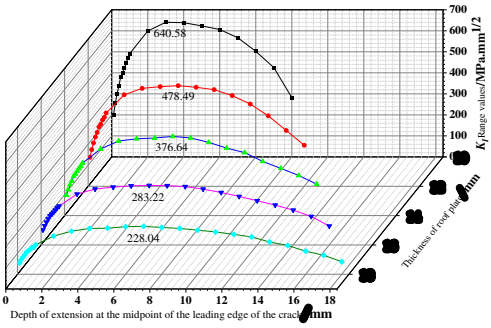

Fig.33 The relationship between the propagation depth at the middle point of crack front and the amplitude of stress intensity factor

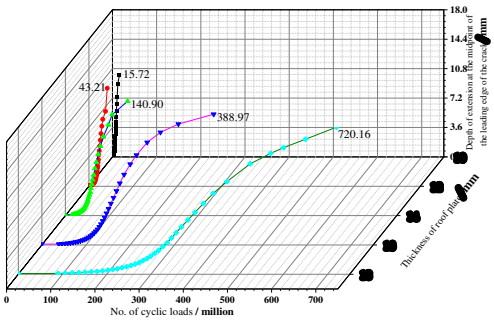

Fig.34 The relationship between the propagation depth at the middle point of crack front and the number of cyclic loading

As can be seen from the above two figures, with the increase of the top plate thickness, the stress intensity factor [7]amplitude at the middle point of the crack leading edge decreases

significantly, and the stress intensity factor amplitude decreases by about 70% when the top plate thickness increases from 10mm to 18mm; with the increase of the top plate thickness the remaining life of the structure becomes longer and longer. An increase in plate thickness, while taking into account economic factors, will greatly help to improve the fatigue life of the structure.

6.5 Thickness of the horizontal partition

The simulation analysis of the test structure is carried out by changing the diaphragm thickness without changing other parameters. The relationship between the propagation depth of the middle point of the crack front and the amplitude of the stress intensity factor(ΔK_I) is shown in Fig.35, and the relationship between the propagation depth of the middle point of the crack front and the number of cyclic loads is shown in Fig.36.

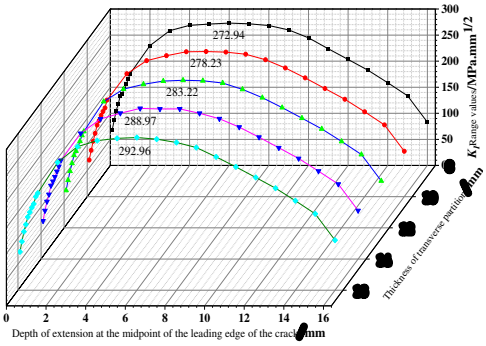

Fig.35 The relationship between the propagation depth at the middle point of crack front and the amplitude of stress intensity factor

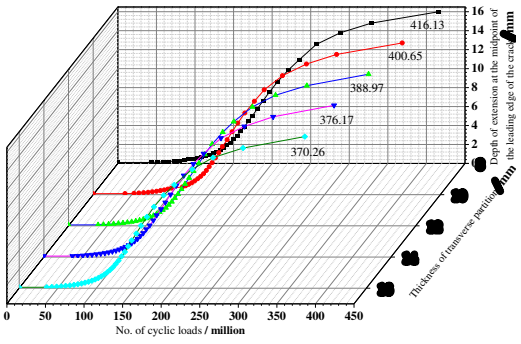

Fig.36 The relationship between the propagation depth at the middle point of crack front and the number of cyclic loading

It can be seen from the above two figures that when the thickness of the diaphragm increases from 8mm to 16mm, the amplitude of the stress intensity factor at the middle point of the crack front does not decrease, but increases, because the change amplitude is relatively small. Therefore, it can be seen that the thickness of the diaphragm has less impact on the service life of the structure.

7. Conclusion

More and more steel bridges for urban rail transport are being built. However, because the vehicle load of rail transit bridge is different from that of highway and railway, the stress characteristics and stress distribution of its OSD structure are also different. Therefore, the research on fatigue of urban rail transit bridge has certain practical and theoretical significance.

In this paper, based on the OSD structure [7]of an urban rail transit cable-stayed bridge, the fatigue test model is designed and carried out. The combination of ABAQUS and Franc3D is used to simulate the fatigue crack growth of the test, the law of the crack growth is studies, and the residual life of the structure is predicted according to the linear elastic fracture mechanics [7]. The main conclusions are the following.

(1) A crack with a length of 15.1cm appears near the boundary of the loading position for the first time after 3million ~ 3.25 million cycles of loading. After 3.25 million ~ 3.5 million cycles of cyclic loading, the crack expanded to 18.6cm in the model test.

(2) The finite element calculation results and the test results are basically the same, so the test can reflect the real state of the model force, and the test data has real reliability.

(3) The type I stress intensity factor of the initial crack is symmetrically distributed and has a large value, with the maximum value reaching 77.67 MPa. $mm^{1/2}$, while the type II and III stress intensity factors fluctuate around 0 MPa. $mm^{1/2}$, and the crack belongs to the crack type dominated by type I cracks.

(4) With the expansion of the crack, the stress intensity factor at the middle point of the leading edge of the crack tends to increase and then decrease. When the size of the short semi-axis of the crack reaches 16 mm, the number of load cycles is nearly 3.9 million. While the number of fatigue cycle loads tested is 3.5 million, with a relative error of 11.4%, which is within an acceptable range.

(5) The increases of U-rib thickness and roof thickness have the positive effect on prolonging the fatigue life of OSD. The influence of roof thickness is particularly significant. When the roof thickness increases from 10mm to 18mm, the amplitude of stress intensity factor decreases by about 70%, which is more helpful to increase the fatigue life.

Compliance with Ethical Standards

The authors declare that there is no potential conflict of interest regarding the publication of this pap er. Research in the paper does not involve human participants or animals. Informed consent is appro ved by all authors of this paper. The supports of the funding are greatly appreciated by authors. The c ontent of the paper belongs to the authors' personal point of view, and does not represent the position of the funding.

Data Availability Statement

All data generated or analyzed during this study are included in this article. All data included in this study are available upon request by contact with the corresponding author.

All authors agree to share the original data of this article. All data generated or analyzed during this study are included in this published article [and its supplementary information files].

These curves are drawn by origin drawing software. Double click the picture to open it. The original data corresponding to the curve can be found in the origin.

Both tables in the manuscript are one of the original data. If a more detailed data analysis process is required, the data sets used and/or analyzed in the current study may be obtained from the corresponding authors as reasonably requested.

Acknowledgments

The supports of the Natural Science Foundation of China (Grant No.51908093), Chongqing Returne d Overseas Scholars' Entrepreneurship and Innovation Support Fund (cx2018113, cx2020117), and National Key Laboratory of Mountain Bridge and Tunnel Engineering Development Fund (CQSLBF −Y14, CQSLBF−Y16−10) are greatly appreciated.

References

[1] Zulie Wu, Sheng Jing, and Junmei Liu. Determination of Fatigue Load for Light Rail Support of Caiyuanba Yangtze Bridge in Chongqing[J]. Advanced Materials Research, 2012, 1615(446):780-785.

[2] Guangliang Bai, Guangwu Tang. Fatigue tests of Overlapping Details for Orthotropic Steel

Bridge Decks and Transverse Beams of Stay Cables[J]. Advanced Materials Research, 2012, 1615(446):3202-3206.
[3] M. C. Baietto, E. Pierres, A. Gravouil, et al. Fretting fatigue crack growth simulation based on a combined experimental and XFEM strategy[J]. International Joumal of Fatigue, 2013, 47:31-43.
[4] Shigenobu Kainuma, Muye Yang, Young-Soo Jeong, et al. Experiment on fatigue behavior of rib-to-deck weld root in orthotropic steel decks[J]. Journal of Constructional Steel Research, 2016,119:113-122.
[5] Samol Ya, Kentaro Yamada, Toshiyuki Ishikawa. Fatigue Evaluation of Rib-to-Deck Welded Joints of Orthotropic Steel Bridge Deck[J]. Journal of Bridge Engineering, 2011, 16(4):492-499.
[6] Yanping Liu, Chuanyao Chen, Guoqing Li. Fatigue Crack Growth and Control of 14MnNbq Welding Plates Used for Bridges[J]. Journal of Engineering Mechanics, 2012, 138(1):30-35.
[7] Yazdani Nur, Albrecht Pedro. Crack Growth Rates of Structural Steel in Air and Aqueous Environments[J]. Engineering Fracture Mechanics, 1989, 32(6):997-1007.
[8] Shiraishi Yuichi,Sakano Masahirro,Sakamoto Chihiro,Konishi Hideyuki,Omori Koichi. Proposal and Verification of Countermeasures against Fatigue Cracking from Weld Joints between Trough Ribs and Cross Ribs in Orthotropic Steel Decks[J]. Procedia Structural Integrity,2022,38:588-595.
[9] Hirai Takahide,Saito Shiro,Sakano Masahiro. Fatigue durability of large-sized trough rib ortho-tropic steel deck for deck crack[J]. ce/papers,2021,4(2-4):1168-1171.
[10] Champenoy Damien,Généreux Grégory,Hajar Ziad,Simon Alain,Fyon Sébastien. Illzach Bridge: Innovative Repair of Orthotropic Deck Using Ultra-High-Performance Fibre-Reinforced Concrete—Return After 5 Years[J]. Structural Engineering International,2020,30(3):387-392.
[11] Rolf Jung Dipl.-Ing.,Tobias Mansperger Dipl.-Ing.. Die Orthoverbund-Fahrbahnplatte[J]. Stahlbau,2020,89(2):129-137.
[12] Andrzej Kasprzak,Andrzej Berger. Strengthening and Widening of Steel Single Box Girder Bridge in Warsaw[J]. Structural Engineering International,2019,29(4):533-536.
[13] Moga Cătălin,PondichiAlb Claudia,Suciu Mircea. Effect of Design Parameters on Shear Lag in Orthotropic Deck of Steel Road Bridges[J]. Bulletin of the Polytechnic Institute of Iaşi. Construction. Architecture Section,2021,67(2):95-104.
[14] Fei Jiang,Bohai Ji,Zhongqiu Fu,Yue Yao. Effect of Weld Profiles on Fatigue Performance of Deck to U-Rib Weld in Orthotropic Steel Deck[J]. Iranian Journal of Science and Technology, Transactions of Civil Engineering,2021(prepublish):1-15.
[15] Cui Chuang,Xu You Lin,Zhang Qing Hua,Wang Feng Yang. Vehicle-induced dynamic stress analysis of orthotropic steel decks of cable-stayed bridges[J]. Structure and Infrastructure Engineering,2020,16(8):1067-1081.
[16] Iqbal Nouman,Fang Heng,Naseem Ahsan,Kashif Muhammad,De Backer Hans. A Numerical Evaluation of Structural Hot-Spot Stress Methods in Rib-To-Deck Joint of Orthotropic Steel Deck[J]. Applied Sciences,2020,10(19):6924-6924.
[17] H. De Backer,A. Outtier,W. Nagy,K. Schotte. Innovative fatigue design of orthotropic steel decks[J]. Bridge Structures,2017,13(2-3):69-80.
[18] Fang Heng,Iqbal Nouman,Van Staen Gilles,De Backer Hans. Experimental and Numerical Investigation of Stress Concentration at Rib-to-Crossbeam Joint[J]. International Journal of Steel Structures,2021,21(1):360-380.

[19] R. Maggenti,S. Shatnawi. Initial and replacement riding surface for the orthotropic San Mateo/Hayward Bridge[J]. Bridge Structures,2017,13(2-3):81-92.
[20] Qu Yu, Zeng Yong, Gu Anbang, Du Baisong. XFEM and its application in fatigue crack growth of orthotropic steel deck [J]. Journal of Chongqing Jiaotong University (Natural Science Edition), 2018,37 (04): 21-27.
[21] Gu Ping, Lu fan, Tang Lin, Li Jianhua. Study on fatigue performance of orthotropic steel deck beams[J]. Structural engineer, 2022,38 (02):99-105.
[22] Tijana Novoselic,Dr.-Ing. Thomas Klähne,Igor Tschepego Dipl.-Ing.,Danny Schönburg,Uwe Heiland Dipl.-Ing.. Neubau einer ÖPNV-Brücke für Straßenbahn, Radfahrer und Fußgänger zum Kienlesberg in Ulm[J]. Stahlbau,2017,86(2):123-138.
[23] Junlin Heng,Kaifeng Zheng,Sakdirat Kaewunruen,Jin Zhu,Charalampos Baniotopoulos. Probabilistic fatigue assessment of rib-to-deck jointsusing thickened edge U-ribs[J]. Steel and Composite Structures,2020,35(6):799-813.
[24] Xiaochen Ju,Kazuo Tateishi. Fatigue Crack Behavior at Rib-To-Deck Weld Bead in Orthotropic Steel Deck[J]. Advances in Structural Engineering,2014,17(10):1459-1468.
[25] Xudong Shao,Dutao Yi,Zhengyu Huang,Hua Zhao,Bin Chen,Menglin Liu. Basic Performance of the Composite Deck System Composed of Orthotropic Steel Deck and Ultrathin RPC Layer[J]. Journal of Bridge Engineering,2013,18(5):417-428.
[26] Zeng Yong, Xue Xiaofang, Zhang Lu, Ao Fuyong. Local stress analysis of new orthotropic steel bridge deck of rail transit[J]. Special structure, 2022,39 (02):73-78.
[27] Alshoaibi Abdulnaser M.. Fatigue crack growth analysis under constant amplitude loading using finite element method[J]. Materials,2022,15(8):2937-2937.
[28] Gudas Claudiu. The effects of fatigue cracks on fastener loads during cyclic loading and on the stresses used for crack growth analysis in classical linear elastic fracture mechanics approaches[J]. Materials Sciences and Applications,2020,11(07):505-551.
[29] A. R. Shahani,M. Babaei. The crack propagation path for a system of surface and subsurface cracks and their interactions due to rolling contact fatigue[J]. Acta Mechanica,2020,231(8):1751-1764.
[30] Robin Andersson,Elena Kabo,Anders Ekberg. Numerical assessment of the loading of rolling contact fatigue cracks close to rail surface irregularities[J]. Fatigue & Fracture of Engineering Materials & Structures,2020,43(5):947-954.

Supplementary Files

This is a list of supplementary files associated with this preprint. Click to download.

- dataavailabilitystatement.docx